ARTICLES
PUBLISHED ONLINE: 25 MAY 2015 | DOI: 10.1038/NMAT4296
nature materials

Selective transformations between nanoparticle superlattices via the reprogramming of DNA-mediated interactions

Yugang Zhang[1], Suchetan Pal[1,2], Babji Srinivasan[3], Thi Vo[2], Sanat Kumar[2] and Oleg Gang[1]*

The rapid development of self-assembly approaches has enabled the creation of materials with desired organization of nanoscale components. However, achieving dynamic control, wherein the system can be transformed on demand into multiple entirely different states, is typically absent in atomic and molecular systems and has remained elusive in designed nanoparticle systems. Here, we demonstrate with *in situ* small-angle X-ray scattering that, by using DNA strands as inputs, the structure of a three-dimensional lattice of DNA-coated nanoparticles can be switched from an initial 'mother' phase into one of multiple 'daughter' phases. The introduction of different types of reprogramming DNA strands modifies the DNA shells of the nanoparticles within the superlattice, thereby shifting interparticle interactions to drive the transformation into a particular daughter phase. Moreover, we mapped quantitatively with free-energy calculations the selective reprogramming of interactions onto the observed daughter phases.

The creation of systems with adaptable and switchable structures is invaluable for achieving dynamic control of material functionality. Systems built from nanoparticles (NPs) often exhibit synergetic and collective properties; thus, regulated transformation of their large-scale organizations could offer a means of switching material properties. Several self-assembly methods, using the particles' sizes[1], charges[2], shapes[3], packing effects[4], polymerization-like growth[5], field-induced assembly[6] and bio-recognition interactions[7–9], have been demonstrated for the creation of NP superlattices, which are the structural basis of designed nanomaterials. If the interparticle molecular linkages are responsive, environmental factors, such as ionic strength[10], pressure[11], or pH (ref. 12), can affect molecular conformations[13], inducing, for instance, a change in interparticle distances. DNA-based approaches, being a powerful strategy for nanomaterial assembly[7,8,14,15], allow alteration of the state of interparticle DNA linkages in highly specific ways. For example, the ability to regulate DNA compact/extended states allows the fabrication of core-satellite nanoparticle clusters with changeable interparticle distances[16], and superlattices with switchable lattice constants[17]. However, it is significantly more challenging to control lattice transitions between different phases, crystallographic symmetries or morphological states, wherein global structural reorganization is required. One tentative example is to exploit peculiar temperature-dependent interactions, such as re-entrant liquid–solid–liquid transitions, as recently studied theoretically[18,19] and experimentally[20,21].

Conceptually, it is exciting to imagine dynamically switchable systems, where a specific structure and the corresponding pathway can be chosen from multiple possible well-defined states, and triggered as desired. Control of system transformations is crucial for creating materials whose functions can be activated on demand. To induce a structural change on a global scale, one requires a significant modification of either particle shape or particle interactions. For example, particle 'shape-shifting' was demonstrated as a means to induce structural transitions[22,23]. However, the experimental realization of phase transformations via interaction- or shape-shifting is challenging, owing to the difficulty in creating suitable and tunable systems permitting crystal-to-crystal transitions while insuring viable kinetic pathways. Here, we demonstrate a novel route for controlling transformations of DNA–NP superlattices into multiple phases via a post-assembly modification of the DNA shells; that is, via the reprogramming of interparticle interactions. By introducing different types of reprogramming DNA strands, we selectively shift the particle–particle interactions, either by increasing both attraction and repulsion, or by separately increasing only attraction or only repulsion. These reprogrammed interactions impose new constraints on particles. Consequently, the lattice can satisfy these constraints only by undergoing a transformation from the original 'mother' phase into one of the 'daughter' states, with the specific end state defined by the reprogrammed interactions. Our experiments show that such selective transformations are fully controlled by the type of input DNA strand; thus, the system's global crystalline structure can be switched on demand via these specific inputs. Using *in situ* measurements, we observed a series of transitions from a CsCl phase to various phases, including CuAu, hexagonal close-packed (HCP), quasi-2D, face-centred cubic (FCC), and a cluster morphology. Moreover, we found that certain daughter phases, such as HCP and quasi-2D, required a mother–daughter pathway and could not be directly assembled from the solution of free NPs and the corresponding strands.

Experimental design and *in situ* structural probing

Our initial system ('mother phase') is built from ~10 nm gold nanoparticles (Au NPs) in a three-step process. First, the Au

[1]Center for Functional Nanomaterials, Brookhaven National Laboratory, Upton, New York 11973, USA. [2]Department of Chemical Engineering, Columbia University, New York, New York 10027, USA. [3]Department of Chemical Engineering, Indian Institute of Technology Gandhinagar, Ahmedabad 682525, India. *e-mail: ogang@bnl.gov

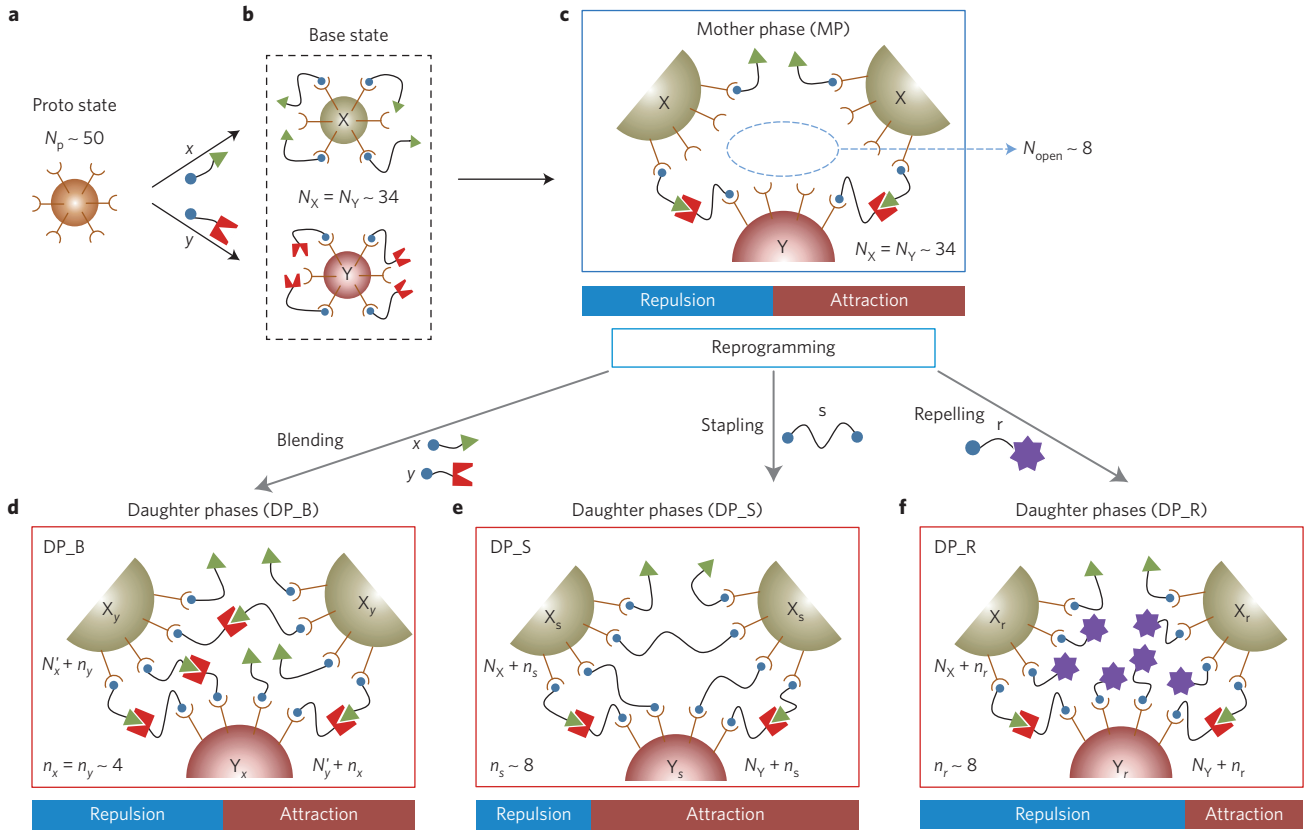

Figure 1 | Illustration of the experimental design for inducing phase transformations in DNA–NP superlattices via selective reprogramming of interparticle interactions, achieved by inputting different types of strands (denoted here as blending, stapling and repelling) that modify the DNA shells of NPs in a lattice. a, The proto-state nanoparticles (NPs) are formed by surface tethering of N_p (~50) proto-DNA strands (see Supplementary Tables 1–3 for the details of DNA designs). **b**, A pair of mutually complementary base-state NPs, X and Y, are created by hybridization of proto-state NP with N_X (~34) of *x* base-DNA strands and N_Y (~34) of *y* base-DNA strands. **c**, Assembly of the mother phase (MP) is achieved by mixing X and Y NPs, and by post-annealing. Owing to the interparticle hybridization of *x* and *y* shells from X and Y NP, respectively, *x* and *y* base-DNA chains change their conformations. As result, there are N_{open} (~8) newly available sites per particle for hybridization of input strands with proto-DNAs (see Supplementary Methods). **d**–**f**, Schematics of phase transformation from MP to one of the daughter phases by the selective modification of DNA shells via reprogramming DNA strands, that is, blending (*x* and *y*), stapling (s), and repelling (r). Accordingly, MP transforms into daughter phases: blending (DP_B) (**d**), stapling (DP_S) (**e**) and repelling (DP_R) (**f**), respectively. During these phase transformations, the particles X(Y) correspondingly hybridize with additional n_y/n_x (or n_x/n_y), n_s and n_r DNA strands. Note: in the case of blending (**d**), N_x (or N_y) changes to N'_x (or N'_y), for example, $N'_x = N_x + n_x$. The complementary shape pairs, shown correspondingly as dots and half circles, or triangles and squares with a triangular dent, represent the complementary DNA base pairs. The notation of subscript for particles, Y_x for instance, indicates a small portion of *x* strands in the shell of a Y NP due to the shell modification with reprogramming strands. On adding the strands to MP, the interparticle repulsion and attraction are changed, as depicted schematically with blue and red bars, respectively, where the bar length represents their strength.

NPs were functionalized with single-strand (ss) DNA (proto-DNA, Supplementary Table 1) into proto-state NPs (Fig. 1a). Second, the proto-state NPs were used to create a pair of complementary X and Y NPs (Fig. 1b), which are able to hybridize with *x* and *y* base-DNA (in analogy to the common chromosome notation). Third, the X and Y NPs were assembled by mixing and subsequently crystallized into a 'mother phase', MP, (Fig. 1c) by annealing at ~31 °C (the melting temperature, $T_m \sim 36$ °C). (See 'Methods' for details.)

We employed synchrotron-based small-angle X-ray scattering (SAXS) for *in situ* probing of NP assemblies. The mother phase exhibits (Fig. 2a, bottom) sharp rings in the 2D SAXS pattern, and the corresponding structure factor $S(q)$ (blue curve) can be indexed as a well-ordered body-centred cubic (BCC) lattice (see Supplementary Methods 'SAXS modelling' for details, Supplementary Fig. 8). The so-formed mother phase is stable over at least several months (Supplementary Fig. 13). However, by introducing the reprogramming strands, we modify the DNA shells of NPs in the mother phase, which shifts the inter-shell interactions, resulting in a lattice transformation, as we discuss below.

Selective lattice transformations by modifying DNA shell

First, we discuss the concept of a dynamically tunable NP shell for programmable phase transformations in the context of DNA–NP assemblies. In contrast to free DNA strands, the interactions of which are mainly governed by sequence-determined Watson–Crick base pairing, the interactions of DNA-coated particles depend on the composition of DNA shells[24–27]. We propose to modulate NP shells in a dynamical fashion when particles are already inter connected in the assembled lattice, by providing different types of input strands that are able to become an integral part of the shell. Depending on the connectivity properties of these inserted strands, shell interactions can be manipulated in desired ways. This reprogramming of interactions can trigger structure transformations.

We hypothesize that the DNA chain configurations on the surface of a free NP are distinct from those between particles in the assembled lattice. For a free unassembled NP, not all proto-strands on the NP surface are able to hybridize with *x* and *y* base-DNA, depending on concentration. Indeed, crowding of single-stranded *x*

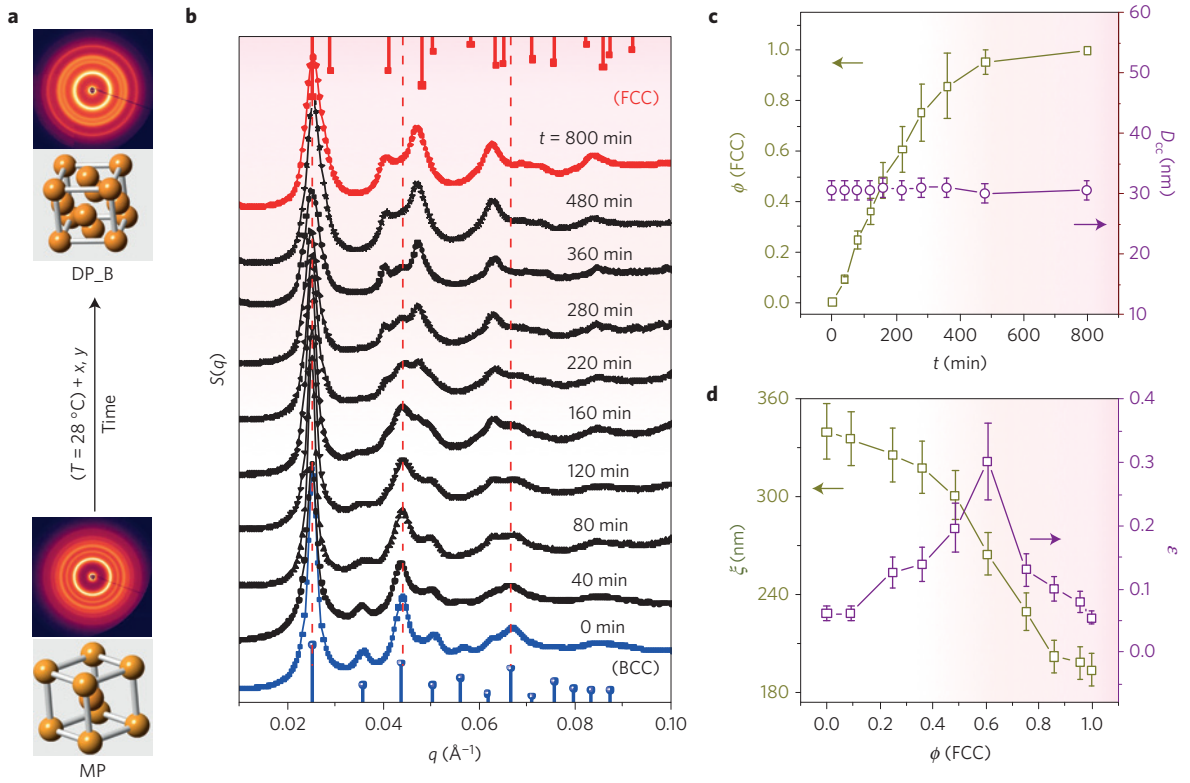

Figure 2 | Transition from mother phase (MP) to daughter phase (DP_B) on introduction of blending strands. a, Scattering patterns and corresponding lattices for the 'mother' phase (MP) and the blending-strands-induced 'daughter' phase (DP_B). **b**, The evolution of *in situ* SAXS measured structure factor, $S(q)$, of MP at 28 °C, after incubation with blending strands (x and y) at room temperature, as shown on Fig. 1. A new DP_B (FCC, indexing is shown at the top) gradually develops from MP (BCC, indexing is shown at the bottom) during an isothermal process ($T = 28$ °C). The detailed two-phase modelling of $S(q)$ is described in Supplementary Methods, and the calculated $S(q)$ are shown in Supplementary Figs 8, 9 and 11a–j for the evolution. **c**, Time-dependent volume fraction (ϕ) of daughter phase (DP_B) and nearest-neighbour centre-to-centre interparticle distance (D_{cc}), extracted from the $S(q)$ fits, are plotted as a function of time during the transition from MP to DP_B (time counting starts when the transition is activated by bringing the system to $T = 28$ °C). **d**, The evolution of the correlation length (ξ) and Williamson Hall slope (ε) as a function of ϕ of DP_B.

and y base-DNA on the NP can partially block the proto-DNA sites, as illustrated in Fig. 1b; there is also an entropy loss for base-DNAs attached to the NP in comparison to their solution state. In contrast, when NPs are assembled in a condensed phase, the proto-DNA sites could be unblocked: the formation of double helix bonds between NPs reduces chain entropy and affects local DNA conformations (see Fig. 1c). These now-opened sites can host the new input strands, which have one end complementary to proto-DNA, while the other end can provide different custom interaction-shifting functions, as we show below. We stress that the only requirement is that certain hybridization/non-hybridization rules should be satisfied; this interaction reprogramming approach does not rely on the use of particular DNA sequences.

To test our hypothesis, we measured the number of proto- (N_p) and base-DNA (N_X or N_Y) on the surface of free particles, as well as the number of available DNA sites in the assemblies (N_{open}). Using a modified reported procedure[28], we found that N_p, N_X and N_{open}, respectively, were ~50, 34 and 8 (see Supplementary Methods, 'DNA number quantification'). Thus, the transition from free NPs to their condensed (aggregated) state, in which DNAs between NPs are hybridized, unblocks about 20–25% of previously unavailable of proto-sites. These sites are used in our study for *in situ* modifications of DNA shells with reprogramming strands. Our study on the kinetics of input strand incorporation within the lattices demonstrated that strand diffusion and hybridization required 2–3 h (Supplementary Fig. 4), which was significantly shorter than our typical incubation time, about 24 h, at room temperature (RT ~ 23 °C).

We explored three types of input reprogramming strands, all of which exerted distinct additional effects on the interparticle interactions: 'blending', 'stapling' and 'repelling', as shown in Fig. 1. The three types of modifications accordingly provide the following interactions: a mixed attraction and repulsion between all particles types ('blending') instead of repulsion-only and attraction-only as in the mother phase; predominant interparticle attraction ('stapling'); and predominant repulsion between neighbouring particles ('repelling'). Although the interaction-shifting does not depend on specific sequences, as long as input DNA strands fulfil their designated roles, the magnitude of the interaction shift may depend on the DNA length[29,30], melting temperature, and the inert DNA tails[31].

Experimentally, for the 'blending' case, we added an equal mixture of x and y DNA strands (x and y) to the solution with the assembled aggregate, and these strands altered the shells of X and Y NPs. As such, both the x and y strands can hybridize randomly with the now unblocked proto-DNA on the surface of the X and Y particles (Fig. 1d), which allows the addition of x onto Y NP and y onto X. This 'blending' results in additional attraction, as well as repulsion, between X(Y) and X(Y) (ref. 27). For the 'stapling' case, the input DNA (s) is designed with both ends complementary to proto-DNA. This design thus increases attraction between next-neighbour NPs, regardless of the particle type (Fig. 1e). Note that the polarity of hybridization of stapling strands with base-DNAs requires folding of stapling linkages (see Supplementary Fig. 5). Finally, 'repelling' (r) DNAs, whose two ends are respectively complementary and

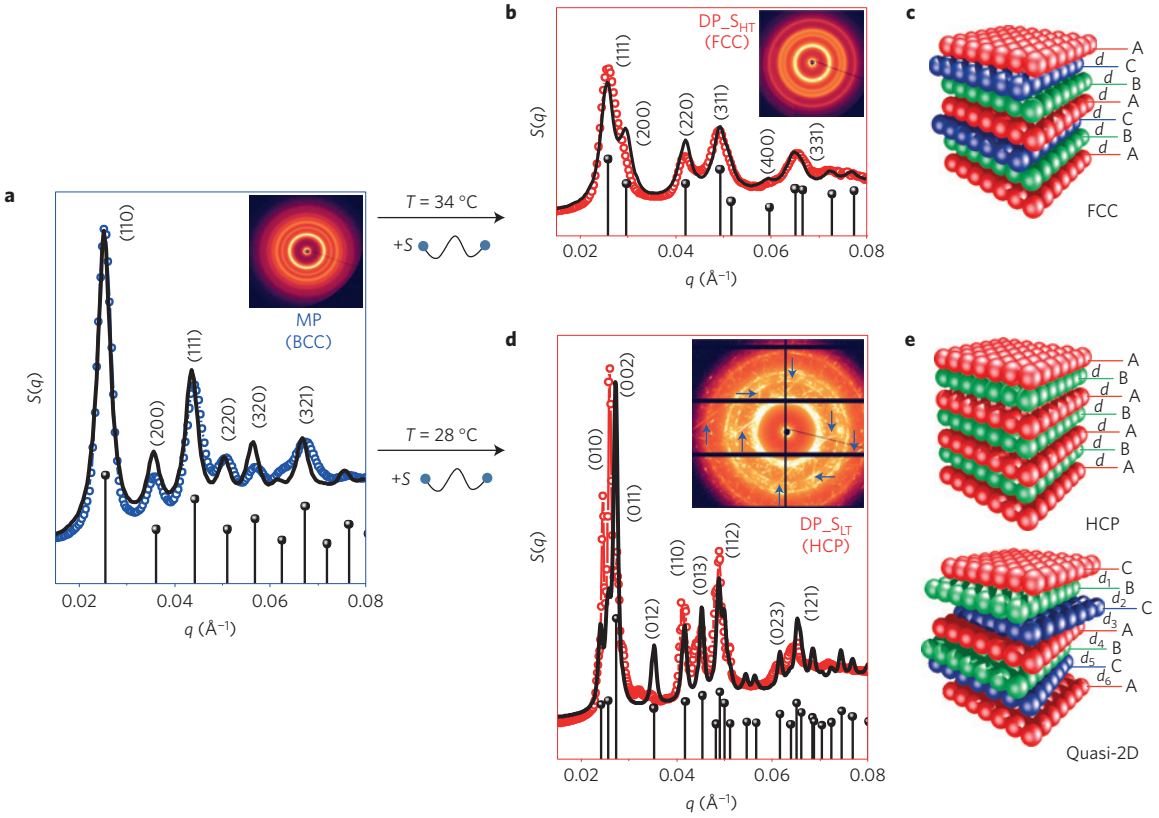

Figure 3 | Transformations induced by stapling strands. a,**b**,**d**, 2D SAXS patterns and the corresponding measured (blue and red circles) and modelled (black lines) structure factors, $S(q)$, for systems with stapling strands from MP (BCC) (**a**) transforming into DP_S_{HT} (FCC) (**b**) at higher annealing T (~34 °C), or into DP_S_{LT} (HCP) (**d**) at lower annealing T (~28 °C). The blue arrows in the DP_S_{LT} pattern highlight the strip features, which signify scattering from 2D crystals. **c**,**e**, Schematics of packing for FCC (ABC periodic layered) (**c**), and HCP (AB periodic layered) and quasi-2D (weakly correlated layered) (**e**) lattices. See Supplementary Methods for the details on the $S(q)$ modelling.

non-complementary to proto-DNA, generate additional repulsion between all next-neighbour particles[24] (Fig. 1f).

Owing to the input of the new types of strands, and some free sites available for DNA hybridization on a particle's surface, certain amounts of these newly added reprogramming strands will be incorporated into the DNA shells of the NPs. We thus denote the shell-modified X and Y particles as X_y and Y_x, X_s and Y_s, and X_r and Y_r, respectively, for 'blending', 'stapling', and 'repelling' input strands. Such targeted-shell modifications can result in phase transformations, as we revealed below. Considering these interaction types, we denote the above three resulting phases respectively as daughter phase blending (DP_B), stapling (DP_S), and repelling (DP_R).

Phase transformation by blending strands

The particle types in the 'mother' phase interact in a well-defined manner: similar particles (XX or YY) repel, and different particles types (XY) attract. However, the input of blending strands modifies these interactions significantly; overall, attraction and repulsion now exist between similar and complementary particles respectively, as schematically shown by the red–blue interaction bar in Fig. 1d. This new interaction scheme can be accommodated only if the superlattice transforms into a different structure. Using *in situ* SAXS measurements, we monitored the transformation in real time, when the system was brought to about 28 °C. Remarkably, we observed (Fig. 2) the 'birth' of a new DP_B phase (T_m ~37 °C), the gradual appearance of which was accompanied by the fading of the mother BCC phase (the modelling is shown in Supplementary Fig. 8), as revealed from the $S(q)$ time evolution (Fig. 2b). The daughter structure shows sharp rings in the 2D pattern (Fig. 2a top). The obtained $S(q)$ (Fig. 2b, red curve) indicates that DP_B is a well-ordered FCC lattice (see Supplementary Fig. 9 for structure modelling). During the BCC-to-FCC transition, the position (q_1) of the first peak in $S(q)$ remains practically unchanged. This implies that the first nearest-neighbour centre-to-centre interparticle distance (D_{cc}) is preserved (Fig. 2c), given the same factor for the position of q_1, $D_{cc} = \sqrt{6}^*\pi/q_1$, for the BCC (diffraction peak 100) and FCC (diffraction peak 111) lattices. Figure 2c depicts the emergence of the daughter phase, whose volume fraction, ϕ (green open squares), gradually increases, as revealed by our SAXS analysis. By fitting the $S(q)$ with a model that accounts for both BCC and FCC phases (see Supplementary Methods and Supplementary Fig. 11a–j), we obtained the time evolution of ϕ. No intermediate phase was observed during this transformation, as indicated by the fits. Such a first-order solid–solid diffusionless transformation from BCC to FCC has been observed for atomic[32] and polymeric systems[33] under a thermal field. A recent study also suggested a similar transition for DNA-coated submicron particles[27], although the transformation was not controlled and the pathway has not been revealed.

Our measurements allow quantification of the transformation pathway by establishing the relationship between the structural correlation length (ξ, a measure of structural order) and the Williamson Hall slope (ε, a relative measure of strain-induced average lattice distortion)[34] with the development of the DP_B (FCC) phase using the data fits (Supplementary Fig. 11a–j). Figure 2d demonstrates that ε first increases by a factor of ~5 until $\phi \sim 0.6$, and then gradually decreases to the initial level of DP_B. This behaviour is possibly caused by the nucleation and growth of FCC 'embryos'; that is, strain develops as domains of the new phase form and expand in

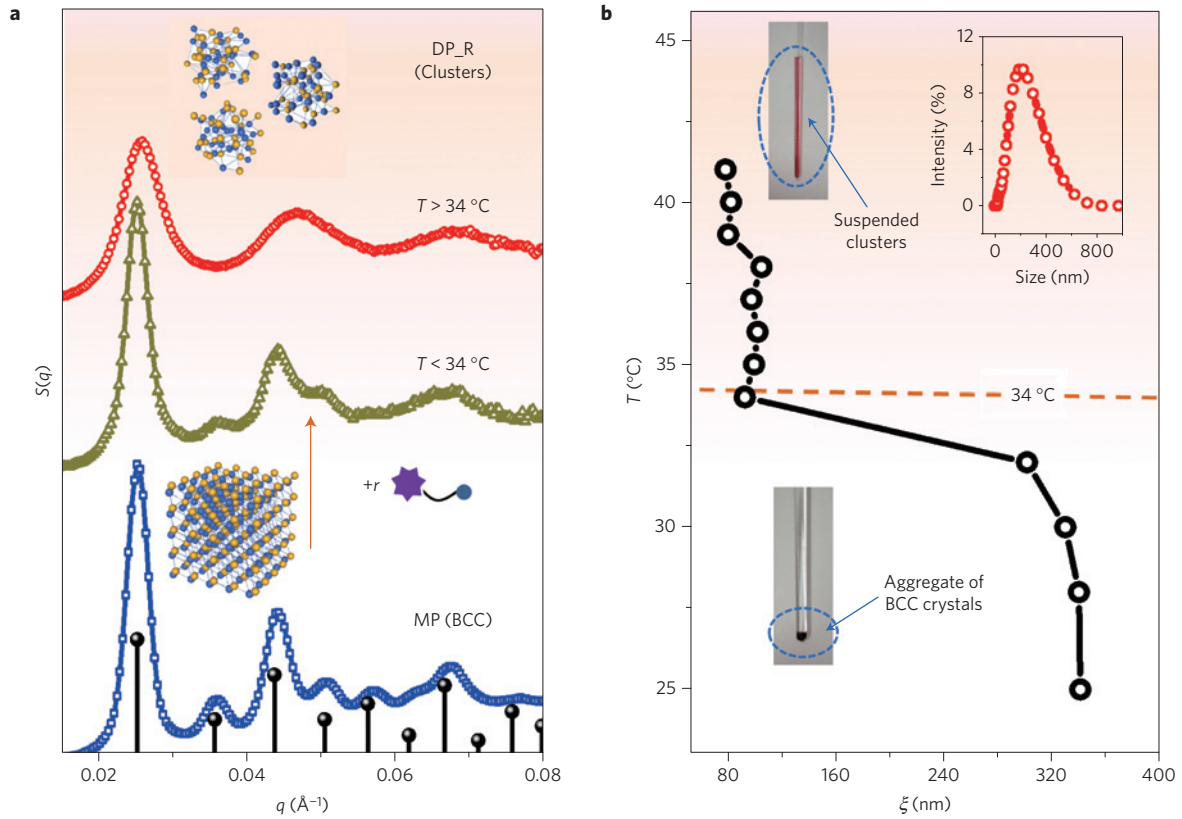

Figure 4 | Morphological transition induced by repelling strands. a, Evolution of room-temperature measured $S(q)$ of MP system (blue points) modified with repelling strand for different annealing temperatures, T. MP (BCC) preserves its structure below 34 °C (yellow points) and develops into a DP_R (cluster) above 34 °C (red points). The inset illustrates the structures of the BCC and cluster phases. The modelled $S(q)$ for the cluster state is shown in Supplementary Fig. 12. **b**, Dependence of the correlation length, ξ, on the annealing temperature, T. The photos (insets) show a precipitated aggregate (polycrystalline) for the BCC phase, in contrast to a suspension for the cluster phase. DLS measurements (inset) show the size distribution of clusters in the suspension.

a matrix of the mother phase. In contrast, ξ monotonically decreases from ~340 nm in the original BCC, to ~200 nm in the FCC, which indicates a modest reduction of grain size.

Compositional order and phase transformation

One of the important characteristics of binary lattices is their compositional order; that is, the degree of particles occupying the 'correct' sites. For example, according to previous studies[7,8,30,35], the MP, comprising two types of particles distinguished by their DNA shells, should form a CsCl-type compositional ordered phase. Recently, it was also shown that the degree of compositional order of CsCl-type NP superlattices was progressively reduced for larger single-stranded DNA shells[30]. It is intriguing to explore how such solid–solid transformation affects the compositional order. Indeed, the binary DP_B could present a compositional disordered FCC, or an ordered CuAu-type lattice.

To examine the compositional order, distinct particle 'colours' (different ability to scatter X-rays) are required. To probe this aspect, we investigated a system consisting of two components with distinctively different X-ray scattering properties; namely, 10 nm Au NPs, and ~6.5 nm CdSe/Te@ZnS quantum dots (QDs) with proto-DNA ~30–40 (see Supplementary Figs 6 and 7 for SEM images). Following the same protocol as for Au–Au systems, we assembled Au and QD into MP (Au–QD MP). The obtained $S(q)$ and the structures are shown in the middle panels of Supplementary Fig. 14a,b. We note a lower degree of crystallinity for the Au–QD system (versus Au–Au), which might arise from the lower number of tethered strands, as well as the slightly ellipsoidal shape and larger size distribution of QDs (ref. 30).

We first confirmed, by modelling of $S(q)$, that the mother phase exhibited compositional order (Supplementary Fig. 14a,b, middle panel). We then verified, using ultraviolet–visible measurements, that no particles were released from the assemblies to the supernatant during the transformation; thus, we concluded that DP_B possesses the same stoichiometry of particles X and Y as in the mother lattice. Consistent with the Au–Au system, the MP of the Au–QD system remained unchanged on temperature annealing if no blending strands (x and y) are added (Supplementary Fig. 14a,b bottom panel). However, Au–QD MP was transformed into a new phase (Supplementary Fig. 14a,b top panel), as indicated by the change of relative positions of the first and second peaks (q_1 and q_2, respectively), on input of x and y strands. Despite the weaker structural order, the value of q_2/q_1 clearly changes from $\sqrt{2}$ (the dashed line in Supplementary Fig. 8b) in MP to $\sqrt{3}$ in DP_B. The first two peaks are indexed as (100) and (110) in BCC-type lattices and as (100) and (111) in FCC-type lattices. The existence of the (100) peaks indicates good compositional order[30] in both structures, implying the formation of CsCl and CuAu lattices (Supplementary Fig. 14). A further structural simulation[36], shown as a solid line in Supplementary Fig. 14a, agrees well with the experimental spectra, using the proposed CsCl- and CuAu-structural models for the corresponding systems.

Polymorphism for transformations by stapling strands

We next investigated the structural transformation of mother phase (BCC, as shown in Fig. 3a) to stapling (DP_S) state on introducing reprogramming strands that increased interparticle attraction regardless of particle types (Fig. 1e). The details of

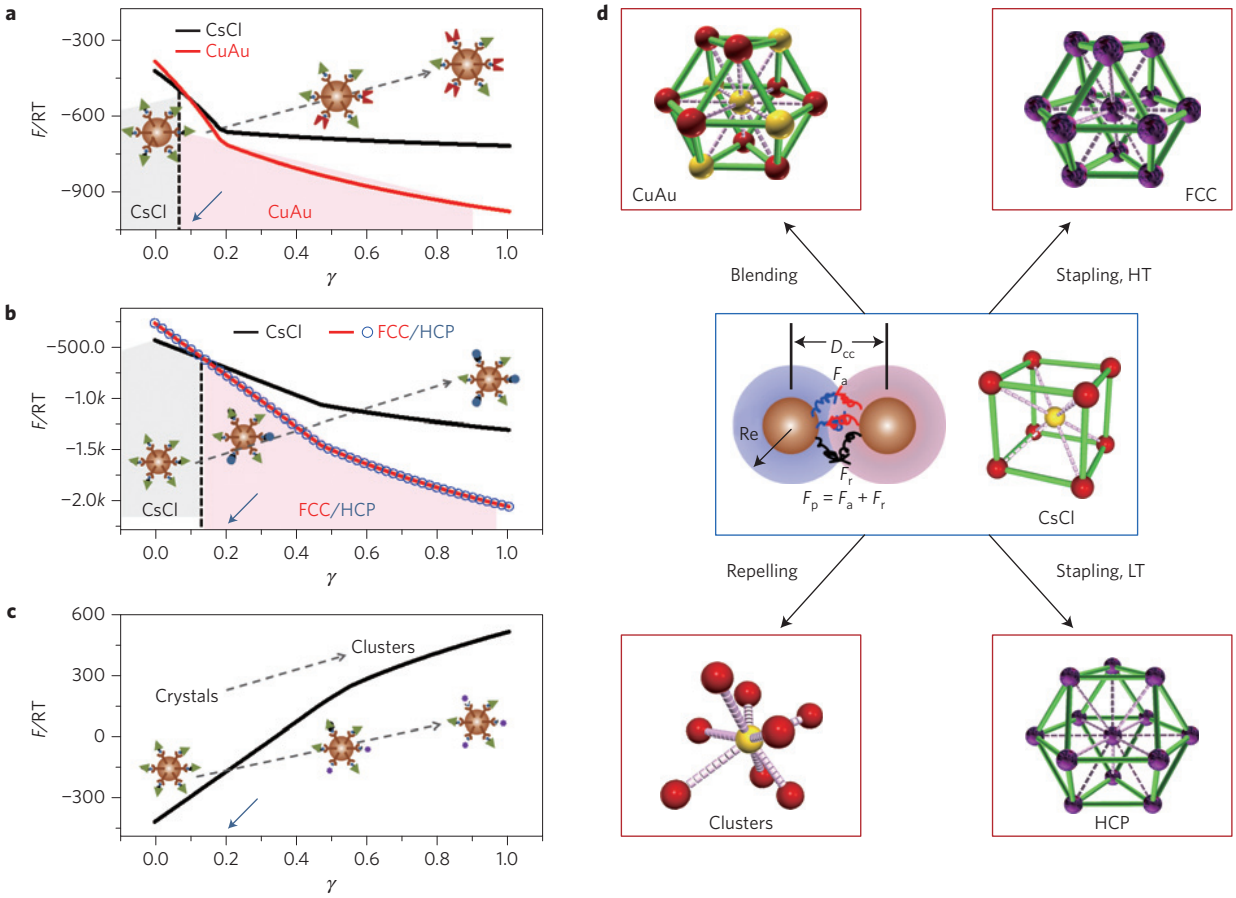

Figure 5 | The effect of input reprogramming strands on interparticle interactions, and on the consequent phase transformation pathways. **a**–**c**, Calculation of free energy (F) for different unit cells as a function of the DNA shell modification parameters (γ), as defined in the text. CsCl and CuAu for the DP_B system (**a**), CsCl and HCP/FCC for the DP_S system (**b**), and CsCl and cluster morphology for the DP_R system (**c**). The γ-dependent (as modified by reprogramming strands) DNA shells are sketched, and the experimental values of γ are shown by blue arrows on the corresponding figures. **d**, Summary of the observed strand-programmable phase transformations from mother phase CsCl to daughter phases, CuAu, FCC, HCP and cluster state; the middle panel also gives the interaction model for a pair of particles.

duplex formation are given in Supplementary Table 3 and depicted in Supplementary Fig. 5. In contrast to the transition induced by blending strands, the DP_S phase does depend on annealing temperature. Figure 3d shows the 2D SAXS pattern and the corresponding $S(q)$ of the new daughter stapling phase. We observed transformation at a higher temperature (∼34 °C, T_m of DP_S ∼39 °C) into an FCC lattice, denoted as DP_S_{HT} (Fig. 3b,c). However, a different phase, denoted as DP_S_{LT}, was found when the transformation occurred at lower temperature (∼28 °C). In this case, an HCP structure emerged, as confirmed by the indexing and modelling (Fig. 3d and Supplementary Fig. 10). Interestingly, the newly formed HCP phase shows grain sizes about four to five times larger than the mother phase. Furthermore, the scattering pattern exhibits strip-like features (indicated by the blue arrows in the top panel in Fig. 3b inset); they indicate the presence of 2D-like crystals in the HCP phase. Owing to a lower temperature of formation, the HCP phase is a kinetically metastable state, as was verified by the further transformation into an FCC phase during annealing at ∼32 °C. Previous simulation work on hard-sphere systems demonstrated a transition from HCP to FCC by the removal of stacking faults as crystals grew larger[37]. The kinetic nature of the observed HCP also agrees with theoretical considerations[38,39] and previous experimental observations[35,40]. Moreover, we obtained similar results for systems with stronger coupling (19-base) between stapling and base-DNA strands versus 14-base in the discussed DP_S system. Interestingly, the system exhibits a phase polymorphism for this transition: both the DP_S_{LT} and DP_S_{HT} phases could only be obtained via the transformation pathway from the MP. These phases could not be assembled from free particles and the corresponding DNAs; namely, proto-state particles mixed with x, y, s strands did not even form an aggregate (Supplementary Fig. 15).

The transition from the BCC to the FCC and HCP phases for stapling scenarios can be understood qualitatively by considering the involved interactions. The stapling strands, by connecting particles irrespective of their types and, thus, increasing interparticle attraction, play a similar role to self-complementary DNA shells, which result in FCC structures as reported[7]. From the viewpoint of crystal structure, the FCC and HCP lattices represent different stacking sequences of hexagonally close-packed layers, AB–AB for HCP and ABC–ABC for FCC (Fig. 3c,e). Owing to the negligible interparticle enthalpy different, and only slightly different entropy[38], it is plausible that a kinetic product, HCP, is formed instead of the FCC phase. Furthermore, in our DNA design, the stapling strand (30 bases) is much shorter than the combined length base-DNAs (58 bases, see Supplementary Fig. 5 for the hybridization scheme), but the hybridization energy between stapling strands and proto-DNA is larger than between the x and y base-DNAs. Therefore, owing to the imposed stress, some bonds between base-DNAs might open when s-DNA is hybridized. As binding between hexagonal layers is weaker than that within a layer (smaller particle-coordination number), some uncorrelated stacking of layers can occur. Recent

computational work predicted the formation of a random HCP (RHCP) structure[41] that was not previously observed. In the extreme case of a full decoupling between layers, and a complete loss of their structural correlation, 2D nanoparticle arrays may be formed; this scenario is possible, given our observations.

Cluster morphology by repelling strands

Finally, we examined the structural reconfiguration induced by a room-temperature incorporation of repelling r strands into the MP lattice; such r strands add a steric interparticle repulsion (Fig. 1f). We brought the modified system to different temperatures to allow for the transformation, and then reduced it back to RT and performed SAXS. On incorporation of r strands at RT, we observed only a moderate change of $S(q)$, indicating a slightly reduced correlation length of the preserved BCC lattice. This behaviour occurred below a transition temperature of about 34 °C, as shown in Fig. 4a (see Supplementary Fig. 16 for details). However, a significant broadening of scattering peaks happened for temperatures >34 °C (Fig. 4a), and persisted even after the sample was cooled to RT. This $S(q)$ change was accompanied by a morphological transition from a condensed aggregate to a suspended phase (DP_R), as apparent from the colour change of the supernatant (photographs Fig. 4b).

We characterized the suspended morphology using dynamic light scattering (DLS), and by modelling the scattering profile (Fig. 4a, red data), as shown in Supplementary Fig. 12. DLS indicates that the suspension consists of clusters with sizes of the order of hundreds of nanometres (around 200 particles per cluster) with a broad size distribution (Fig. 4b inset and Supplementary Fig. 17). We compare the temperature dependence of the correlation length $\xi(T)$ in Fig. 4b with DLS results and macroscopic observations. When r strands are added, an abrupt ξ decrease occurs, from about 300 nm to 90 nm, at the transition temperature. We propose that the incorporation of r strands in a shell imposes only internal pressure due to steric effects, but the lattice remains intact because of x–y linkages between NP shells. However, close to the transition temperature those interparticle bridges (between x base-DNA and y base-DNA linkages) start to partially melt; consequently, lattice order is decreased. When the temperature is reduced back to RT, particles cannot form a continuous phase owing to the steric repulsion of r strands. Instead, a cluster state is formed as a compromise to satisfy some x–y hybridizations. $S(q)$ reveals (Fig. 4) a similar position (q_1) of the first scattering peak for mother BCC and daughter cluster morphology. As the interparticle distances for those two cases are determined by a similar prefactor, that is, $D_{cc} = \sqrt{6} \times \pi/q_1$ for BCC and $D_{cc} = 2.45 \times \pi/q_1$ (ref. 42) for the unstructured cluster, we conclude that the transition does not affect interparticle distances. The repelling interaction, due to its steric nature, can be further modulated by changing the length of r strands. For example, we found that to induce such a BCC-to-cluster transition, longer (30-base) tails were required; a short tail (20-base) resulted only in a subtle structural change of the mother BCC lattice.

Modelling of input-strands-induced interaction shifting

We further established a quantitative relationship between the different types of input reprogramming strands, and the modification of interparticle interactions that led to the observed transformations. Our calculations were carried out in three steps; namely, interactions parameterization, pair-interactions modelling, and lattice free-energy calculation (see Supplementary Information 'Interparticle interactions', Supplementary Figs 18 and 19 and Supplementary Table 3, for details of the calculation). First, we parameterized our DNA shell components using a shell modification factor (γ), which was defined as the number ratio of strands that were different-to-particle (for example, x to Y) to strands that were same-to-particle (for example, x to X). For instance, one computes $\gamma = 0$ for a shell with one component and $\gamma \sim 0.24$ (=8/34) for the repelling case. Thus, a larger γ indicates a higher degree of shell modification. The γ-dependent DNA shells in systems DP_B, DP_S and DP_R accordingly are depicted in Fig. 5a–c, where the corresponding γ values are estimated from the experimental data as ~0.11, 0.24 and 0.24, respectively. Second, we developed a DNA-shell interaction model for a two-particle system, and calculated the free energy based on the derived canonical partition function. Third, the free energy of a lattice unit cell was calculated as a function of structure symmetry and lattice parameters.

The calculation results for pathways from mother phase to different daughter phases (DP_B, DP_S, and DP_R) are shown in Fig. 5a–c. As our BCC is actually a binary lattice with respect to surface-attached DNA, namely a CsCl lattice, we calculated the energy for CsCl rather than that of mono-component BCC. In the case of for the blending daughter phase (DP_B), the AuCu lattice becomes energetically favourable over CsCl when $\gamma > \sim 0.1$, which is comparable to the experimental value of $\gamma \approx 0.11$, and, thus, explains the stable AuCu phase (Figs 2, 3 and 5d top left). The calculation for the stapling daughter phase (DP_S) reveals that FCC and HCP are energetically indistinguishable in our model; however, the hydrodynamic correlation movements between particles[41] might play a role in the observed formation of temperature-dependent phases. Nevertheless, the results show that both phases are more favourable than CsCl at $\gamma > \sim 0.14$. Hence, our experimental $\gamma \approx 0.24$ supports the dominance of the FCC or HCP over the CsCl phase. As for the repelling daughter phase (DP_R), our model shows that repulsion energy (F_r) exceeds attraction energy (F_a) at $\gamma \approx 0.3$; therefore, the assemblies will dissociate on such shell modification. For our experimental case, the modification of DNA shells by r strands results in $|F_r/F_a| \sim 0.7$ and $\gamma \approx 0.24$, which are indicative of lattice destabilization and a transition to a cluster morphology (Figs 4 and 5d bottom left).

In summary, we have demonstrated the selective transformations of DNA–nanoparticle superlattices into distinctive structures by introducing specific types of strands that modify interparticle interactions within the lattice. We have related quantitatively the DNA-induced interaction-shifting and the resultant phases. The demonstrated dynamic switching of the entire superlattice will allow the creation of reprogrammable and switchable materials, wherein multiple states can be activated to enable different functional properties. Furthermore, the common susceptibility to the genetic input of the nanoparticle-based materials discussed herein and of living matter might open intriguing routes for dynamical interfacing between biological and man-made systems. The presented concept might also open possibilities for creating DNA-based nanoscale materials that are 'genetically' modifiable and can undergo structural 'evolution'.

Methods

Methods and any associated references are available in the online version of the paper.

Received 30 January 2015; accepted 16 April 2015; published online 25 May 2015

References

1. Redl, F. X., Cho, K. S., Murray, C. B. & O'Brien, S. Three-dimensional binary superlattices of magnetic nanocrystals and semiconductor quantum dots. *Nature* **423,** 968–971 (2003).
2. Kostiainen, M. A. *et al.* Electrostatic assembly of binary nanoparticle superlattices using protein cages. *Nature Nanotech.* **8,** 52–56 (2013).
3. Glotzer, S. C. & Solomon, M. J. Anisotropy of building blocks and their assembly into complex structures. *Nature Mater.* **6,** 557–562 (2007).
4. Damasceno, P. F., Engel, M. & Glotzer, S. C. Predictive self-assembly of polyhedra into complex structures. *Science* **337,** 453–457 (2012).

5. Liu, K. *et al.* Step-growth polymerization of inorganic nanoparticles. *Science* **329,** 197–200 (2010).
6. Yan, J., Bloom, M., Bae, S. C., Luijten, E. & Granick, S. Linking synchronization to self-assembly using magnetic Janus colloids. *Nature* **491,** 578–581 (2012).
7. Park, S. Y. *et al.* DNA-programmable nanoparticle crystallization. *Nature* **451,** 553–556 (2008).
8. Nykypanchuk, D., Maye, M. M., van der Lelie, D. & Gang, O. DNA-guided crystallization of colloidal nanoparticles. *Nature* **451,** 549–552 (2008).
9. Geerts, N. & Eiser, E. DNA-functionalized colloids: Physical properties and applications. *Soft Matter* **6,** 4647–4660 (2010).
10. Xiong, H. M., Sfeir, M. Y. & Gang, O. Assembly, structure and optical response of three-dimensional dynamically tunable multicomponent superlattices. *Nano Lett.* **10,** 4456–4462 (2010).
11. Srivastava, S., Nykypanchuk, D., Maye, M. M., Tkachenko, A. V. & Gang, O. Super-compressible DNA nanoparticle lattices. *Soft Matter* **9,** 10452–10457 (2013).
12. Roiter, Y., Minko, I., Nykypanchuk, D., Tokarev, I. & Minko, S. Mechanism of nanoparticle actuation by responsive polymer brushes: From reconfigurable composite surfaces to plasmonic effects. *Nanoscale* **4,** 284–292 (2012).
13. Tokarev, I. & Minko, S. Tunable plasmonic nanostructures from noble metal nanoparticles and stimuli-responsive polymers. *Soft Matter* **8,** 5980–5987 (2012).
14. Knorowski, C., Burleigh, S. & Travesset, A. Dynamics and statics of DNA-programmable nanoparticle self-assembly and crystallization. *Phys. Rev. Lett.* **106,** 215501 (2011).
15. Halverson, J. D. & Tkachenko, A. V. DNA-programmed mesoscopic architecture. *Phys. Rev. E* **87,** 062310 (2013).
16. Sebba, D. S., Mock, J. J., Smith, D. R., LaBean, T. H. & Lazarides, A. A. Reconfigurable core-satellite nanoassemblies as molecularly-driven plasmonic switches. *Nano Lett.* **8,** 1803–1808 (2008).
17. Maye, M. M., Kumara, M. T., Nykypanchuk, D., Sherman, W. B. & Gang, O. Switching binary states of nanoparticle superlattices and dimer clusters by DNA strands. *Nature Nanotech.* **5,** 116–120 (2010).
18. Russo, J., Tavares, J. M., Teixeira, P. I. C., da Gama, M. M. T. & Sciortino, F. Re-entrant phase behaviour of network fluids: A patchy particle model with temperature-dependent valence. *J. Chem. Phys.* **135,** 034501 (2011).
19. Angioletti-Uberti, S., Mognetti, B. M. & Frenkel, D. Re-entrant melting as a design principle for DNA-coated colloids. *Nature Mater.* **11,** 518–522 (2012).
20. Feng, L., Laderman, B., Sacanna, S. & Chaikin, P. Re-entrant solidification in polymer–colloid mixtures as a consequence of competing entropic and enthalpic attractions. *Nature Mater.* **14,** 61–65 (2015).
21. Rogers, W. B. & Manoharan, V. N. Programming colloidal phase transitions with DNA strand displacement. *Science* **347,** 639–642 (2015).
22. Zhang, Y. G., Lu, F., van der Lelie, D. & Gang, O. Continuous phase transformation in nanocube assemblies. *Phys. Rev. Lett.* **107,** 135701 (2011).
23. Nguyen, T. D., Jankowski, E. & Glotzer, S. C. Self-assembly and reconfigurability of shape-shifting particles. *ACS Nano* **5,** 8892–8903 (2011).
24. Maye, M. M., Nykypanchuk, D., van der Lelie, D. & Gang, O. DNA-Regulated micro- and nanoparticle assembly. *Small* **3,** 1678–1682 (2007).
25. Nykypanchuk, D., Maye, M. M., van der Lelie, D. & Gang, O. DNA-based approach for interparticle interaction control. *Langmuir* **23,** 6305–6314 (2007).
26. Dreyfus, R. *et al.* Simple quantitative model for the reversible association of DNA coated colloids. *Phys. Rev. Lett.* **102,** 048301 (2009).
27. Casey, M. T. *et al.* Driving diffusionless transformations in colloidal crystals using DNA handshaking. *Nature Commun.* **3,** 1209 (2012).
28. Demers, L. M. *et al.* A fluorescence-based method for determining the surface coverage and hybridization efficiency of thiol-capped oligonucleotides bound to gold thin films and nanoparticles. *Anal. Chem.* **72,** 5535–5541 (2000).
29. Xiong, H. M., van der Lelie, D. & Gang, O. Phase behavior of nanoparticles assembled by DNA linkers. *Phys. Rev. Lett.* **102,** 015504 (2009).
30. Zhang, Y. G., Lu, F., Yager, K. G., van der Lelie, D. & Gang, O. A general strategy for the DNA-mediated self-assembly of functional nanoparticles into heterogeneous systems. *Nature Nanotech.* **8,** 865–872 (2013).
31. Di Michele, L. *et al.* Effect of inert tails on the thermodynamics of DNA hybridization. *J. Am. Chem. Soc.* **136,** 6538–6541 (2014).
32. Sandoval, L., Urbassek, H. M. & Entel, P. The Bain versus Nishiyama–Wassermann path in the martensitic transformation of Fe. *New J. Phys.* **11,** 103027 (2009).
33. Bang, J., Lodge, T. P., Wang, X. H., Brinker, K. L. & Burghardt, W. R. Thermoreversible, epitaxial fcc↔bcc transitions in block copolymer solutions. *Phys. Rev. Lett.* **89,** 215505 (2002).
34. Williamson, G. K. & Hall, W. H. X-Ray line broadening from filed aluminium and wolfram. *Acta Metall. Mater.* **1,** 22–31 (1953).
35. Macfarlane, R. J. *et al.* Nanoparticle superlattice engineering with DNA. *Science* **334,** 204–208 (2011).
36. Yager, K. G., Zhang, Y. G., Lu, F. & Gang, O. Periodic lattices of arbitrary nano-objects: Modeling and applications for self-assembled systems. *J. Appl. Crystallogr.* **47,** 118–129 (2014).
37. Pronk, S. & Frenkel, D. Can stacking faults in hard-sphere crystals anneal out spontaneously? *J. Chem. Phys.* **110,** 4589–4592 (1999).
38. Woodcock, L. V. Entropy difference between the face-centred cubic and hexagonal close-packed crystal structures. *Nature* **385,** 141–143 (1997).
39. Mau, S. C. & Huse, D. A. Stacking entropy of hard-sphere crystals. *Phys. Rev. E* **59,** 4396–4401 (1999).
40. Hoogenboom, J. P., Derks, D., Vergeer, P. & van Blaaderen, A. Stacking faults in colloidal crystals grown by sedimentation. *J. Chem. Phys.* **117,** 11320–11328 (2002).
41. Jenkins, I. C., Casey, M. T., McGinley, J. T., Crocker, J. C. & Sinno, T. Hydrodynamics selects the pathway for displacive transformations in DNA-linked colloidal crystallites. *Proc. Natl Acad. Sci. USA* **111,** 4803–4808 (2014).
42. Warren, B. E. X-Ray determination of the structure of glass (reprint). *J. Am. Ceram. Soc.* **75,** 5–10 (1992).

Acknowledgements

We thank K. Yager, V. Venkatasubramanian and L. Wu for helpful discussions. We thank F. Lu for help with DLS and DNA hybridization kinetics measurements. Research carried out at the Center for Functional Nanomaterials and National Synchrotron Light Source, Brookhaven National Laboratory, is supported by the US Department of Energy, Office of Basic Energy Sciences, under Contract No. DE-SC0012704. Research at Columbia University was supported by the US Department of Energy, Office of Basic Energy Sciences, Division of Materials Sciences and Engineering under Award DE-FG02-12ER46909.

Author contributions

Y.Z. and O.G. conceived the concept and designed the experiments. Y.Z. performed the experiments and analysed the data. S.P. contributed to the measurements. O.G. contributed to the data analysis. Y.Z., B.S., T.V. and S.K. contributed to modelling the particle interactions. Y.Z. and O.G. wrote the paper. O.G. supervised the project. All authors discussed the results and commented on the manuscript.

Additional information

Supplementary information is available in the online version of the paper. Reprints and permissions information is available online at www.nature.com/reprints. Correspondence and requests for materials should be addressed to O.G.

Competing financial interests

The authors declare no competing financial interests.

Methods

Assembly of DNA functionalized gold nanoparticles into 'mother phase'. Our initial system ('mother phase') is built from ~10 nm gold nanoparticles (Au NPs) in a three-step process. First, we synthesized the building blocks (Au NPs), and attached 30-base single-strand (ss) DNA (ref. 8; Supplementary Table 1) to their surfaces; these are correspondingly denoted as proto-state NPs (Fig. 1a) and proto-DNA. Second, we generated base-state NP by hybridizing proto-state NP with base-DNA (Fig. 1b). The proto-state NPs (in 140 mM NaCl phosphate buffer) were split into two portions, and correspondingly hybridized (Fig. 1b) with the *x* and *y* base-DNA (in analogy to the common chromosome notation) to produce X and Y NP. The *x* and *y* strands contain the same 20-base sequence at their ends, which are complementary to the NP-tethered proto-DNA, while the other 8-base ends of *x* and *y* are mutually complementary. After purifying the excess DNA, we obtained a set of complementary particles (X and Y), denoted as base-state NPs (hydrodynamic radius $R_e \sim 18$ nm, Supplementary Fig. 17). Third, we assembled the mother system by combining equivalent amounts of complementary particles X and Y. The assembly was crystallized further into a mother phase, MP, (Fig. 1c) by annealing at ~31 °C (the melting temperature, $T_m \sim 36$ °C).

Phase transformations of 'mother phase' by using DNA strands as input. Different types of DNA strands were introduced into the solution with the assembled 'mother phase'. The *in situ* structure evolution as a function of temperature and time was monitored. (See 'Selective lattice transformations' for details.)

Characterization of nanoparticles and assemblies. The morphology of nanoparticles was characterized by electron microscopy. The number of proto-DNA, base-DNA and the incorporated input DNA were determined based on the reported fluorescence-based method. Synchrotron-based SAXS (NSLS X-9) was employed to probe the *in situ* structure of particle assemblies. (See Supplementary Methods and 'DNA number quantification' for details.)

Modelling of SAXS profiles and interparticle interactions. To simulate powder SAXS profiles, based on our previous work[30,36], we developed a scattering formalism, which accounted for particle size, polydispersity, lattice disorder and micro-strain, and average grain size, for single-phase, binary-phase and cluster systems. For a quantitative understanding of the input-DNA-induced phase transformations, we developed a pairwise DNA-shell interaction model based on the reported[26,35] and calculated free energy between a pair of particles, and then calculated the free energy in different crystal structures. (See Supplementary Information 'SAXS' and 'Calculation of interparticle interactions' for details.)